WELDING RESEARCH

SUPPLEMENT TO THE *WELDING JOURNAL*, JULY 1996
Sponsored by the American Welding Society and the Welding Research Council

Physical Modeling of Nitrogen Partition between the Weld Metal and Its Plasma Environment

A plasma near the weld pool creates a condition where the concentration of nitrogen in the weld metal exceeds equilibrium Sieverts' Law calculations, and a model is applied to explain this phenomenon

BY T. A. PALMER AND T. DEBROY

ABSTRACT. When pure iron is exposed to diatomic nitrogen, the equilibrium concentration of nitrogen in iron can be determined from Sieverts' Law. However, during many fusion welding processes, a plasma, consisting of various excited species, atoms, ions, and electrons, is present near the weld pool and affects the dissolution process. Sieverts' Law, therefore, cannot be applied to understand the dissolution of nitrogen during welding of steels. The work reported here is aimed at understanding the basic laws governing the partition of nitrogen between the weld metal and its plasma environment.

To avoid temperature gradients on the weld pool surface and spatially variable properties of the plasma in the gas phase, small high-purity iron samples, maintained at a constant temperature, were exposed to a number of low-pressure nitrogen plasmas and analyzed for the resulting nitrogen contents. Throughout the range of experimental conditions, the concentration of nitrogen in each iron sample was significantly higher than the Sieverts' Law predictions. Nitrogen-containing plasmas were characterized using optical emission spectroscopy to examine the species present and determine electron temperature. Thermodynamic calculations show that a trace amount of monatomic nitrogen in the plasma causes a many-fold increase in the nitrogen solubility above that predicted by Sieverts' Law. The experimental results are explained on the basis of a model involving the dissociation of diatomic nitrogen in the plasma and subsequent dissolution of atomic nitrogen in iron. The applicability of the results of the physical modeling experiments to GTA welding of iron is demonstrated.

T. A. PALMER and T. DEBROY are with Department of Materials Science and Engineering, The Pennsylvania State University, University Park, Pa.

Introduction

At the high temperatures characteristic of welding, the rates of reaction between oxygen and nitrogen and the weld metal are rapid. The weld metal is protected from exposure to these gases by a number of shielding methods. Shielding may be achieved by means of a flux as in electroslag welding; an external gas supply like that used in gas metal arc (GMA), gas tungsten arc (GTA), and plasma welding; a combination of the two as in shielded metal arc (SMA) welding; or from the evacuation of the atmosphere as in electron beam welding. In the welding of reactive metals, special shielding measures such as welding inside a gas-filled box are often used to protect the weld metal. Without the benefit of shielding effects, oxygen and nitrogen contents as high as 0.7 and 0.2 wt-%, respectively, have been obtained in steel welds during arc welding (Ref. 1). These concentration levels are far greater than those in the base and filler metals and indicate the importance of the dissolution of these species into the metal from the gas phase. Since the presence of nitrogen, oxygen, and hydrogen in the weld metal affects its properties, the control of concentration of these elements in steel weldments is an important goal.

At a constant temperature, the equilibrium concentration of nitrogen in iron is given by Sieverts' Law, which states that the equilibrium nitrogen concentration in iron is proportional to the square root of the partial pressure of diatomic nitrogen (Ref. 2):

$$\frac{1}{2}N_2(g) \rightarrow \underline{N}(wt\ \%) \qquad (1)$$

KEY WORDS

Diatomic Nitrogen
Sieverts' Law
Weld Metal
Nitrogen Dissolution
Plasma
Arc Atmosphere
Equilibrium
GTA Welding

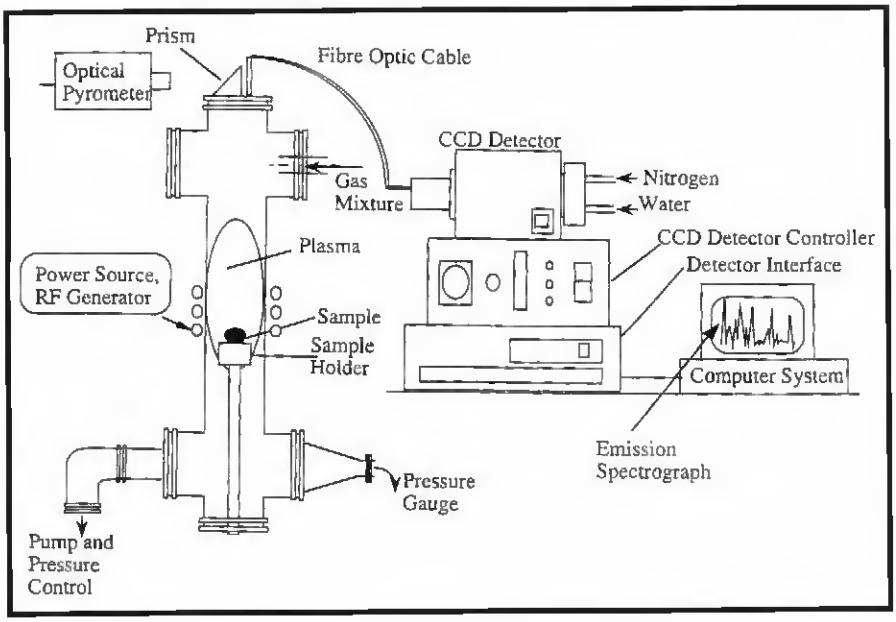

Fig. 1 — Schematic diagram of the experimental setup.

$$\underline{N}(wt\ \%) = K^{d}_{eq}\sqrt{P_{N_2}} = \sqrt{P_{N_2}}\, e^{\frac{\Delta G^{o}_{1}}{RT}} \qquad (2)$$

where ΔG_1^o is the standard free energy for reaction 1, $\underline{N}$(wt-%) is the nitrogen concentration in solution at equilibrium with the diatomic nitrogen gas, K^d_{eq} is the equilibrium constant for reaction 1, P_{N2} is the partial pressure of N_2, and T is the temperature of iron. During fusion welding processes such as laser, arc, and electron beam welding, a plasma phase resides above the weld pool. The plasma consists of electrons, ions, excited atoms, and molecules and can collectively be both electrically conducting and neutral. When a diatomic gas is transformed to a plasma phase, it may dissociate, ionize, or become electrically or vibrationally excited. Each of these individual species will then have different equilibria with the metal. As a result, Sieverts' Law cannot be applied to understand the dissolution of diatomic gas species into a metal in contact with a plasma. In many welding processes, the weld metal comes into contact with a plasma formed from a diatomic source gas.

Several investigators have reported that the solubility of diatomic gaseous species in metals is enhanced above that predicted by Sieverts' Law when a plasma is present above the liquid melt (Refs. 3–9). Ohno, *et al.* (Ref. 3), and Uda, *et al.* (Ref. 4), have shown that the concentrations of nitrogen in liquid nickel and iron during arc melting are significantly higher than the corresponding equilibrium solubilities when the metals are exposed to diatomic nitrogen under non-arc melting conditions. Katz and King (Ref. 5) observed that, in the presence of an arc discharge, the concentration of nitrogen in liquid iron was significantly higher than the value predicted by Sieverts' Law. Bandopadhyay, *et al.* (Ref. 6), studied the plasma enhanced nitrogen solubility in pure tantalum and niobium at 2243 K and attributed the enhanced nitrogen solubility to the presence of atomic nitrogen in the plasma. Ouden and Griebling (Ref. 7) found that the solubility of nitrogen in pure iron in the presence of an arc was much greater than that calculated by Sieverts' Law. Lakomskii and Torkhov (Ref. 8) attributed the plasma enhanced solubility of nitrogen in metals to excited nitrogen molecules, N^*_2. On the other hand, Gedeon and Eagar (Ref. 9) explained the enhanced hydrogen concentration in the weld metal by assuming the presence of monatomic hydrogen in the gas phase.

Each of these theories can be applied to the explanation of the enhanced nitrogen solubility and is summarized below. The first theory involving the dominant

Fig. 2 — Photograph of a representative glow discharge plasma created with the experimental setup.

Table 1 — Comparison of Several Important Features of Plasmas Formed during Common Welding Processes and a Glow Discharge Plasma

Feature	Electric Arc	Laser/Electron Beam	Glow Discharge Plasma
Species in the Gas Phase	Electrons, Ions (N_2^+, N^+), Excited Neutral Atoms and Molecules (N^*, N^*_2), and Monatomic and Diatomic Species (N, N_2)	Electrons, Ions (N_2^+, N^+), Excited Neutral Atoms and Molecules (N^*, N^*_2), and Monatomic and Diatomic Species (N, N_2)	Electrons, Ions (N_2^+, N^+), Excited Neutral Atoms and Molecules (N^*, N^*_2), and Monatomic and Diatomic Species (N, N_2)
Typical Electron Energy (K)	6000–16000 (Ref. 27)	3400–17000 (Ref. 14 and 31)	4000–13500 (This work and Ref. 26)
Typical Electron Density (m^{-3})	10^{21}–10^{23} (Ref. 25)	10^{20}–10^{24} (Ref. 29 and 30)	10^{13}–10^{20} (Ref. 25 and this work)
Temperature Gradient on Metal Surface	Present, Strong	Present, Strong	Absent
Energy Density during Welding	Medium	High	Low

role of activated nitrogen molecules (Ref. 8) in the plasma is described by Equations 3–6.

$$N_2^* + Site \rightarrow N_2^*(ads) \quad (3)$$

$$N_2^*(ads) + Site \rightarrow 2N(ads) \quad (4)$$

$$\underline{2N(ads) \rightarrow 2\underline{N}(\%) + 2Sites} \quad (5)$$

$$N_2^*(g) \rightarrow 2N(\%) \quad (6)$$

where N^*_2 represents nitrogen molecules with excess vibrational energy provided by the electric field. The second theory describing the dominant role of monatomic nitrogen (Ref. 5) in the reaction is displayed in Equations 7–9.

$$N(g) + Site \rightarrow N(ads) \quad (7)$$

$$\underline{N(ads) \rightarrow \underline{N}(\%) + Site} \quad (8)$$

$$N(g) \rightarrow \underline{N}(wt\ \%) \quad (9)$$

Although the enhanced dissolution process is consistent with each of these theories, no unified theory for the quantitative understanding of the extent of enhanced dissolution has emerged up to this point.

The transformation of diatomic molecules to excited neutral atoms and ions in the gas phase involves inelastic collisions of the diatomic molecules with electrons (Ref. 6). Plasma properties such as the electron density and energy affect the formation of various atomic, ionic, and excited neutral species from the diatomic molecules. Determination of the nature of the plasma and the concentration of various species within the plasma is the key to a quantitative understanding of the

Table 2 — Free Energy Relationships for Nitrogen Solubility Calculations in γ-Fe (1184 K to 1669 K).

Reaction	Free Energy-Temperature Relationship (cal/mol)	Reference Number
$\frac{1}{2}N_2(g) \rightarrow N(g)$	86,596.0 – 15.659 T	12
$\frac{1}{2}N_2(g) \rightarrow N$(wt-%)	−2060 + 8.94 T	13
$N(g) \rightarrow N$(wt-%)	−88,656 + 24.599 T	12, 13

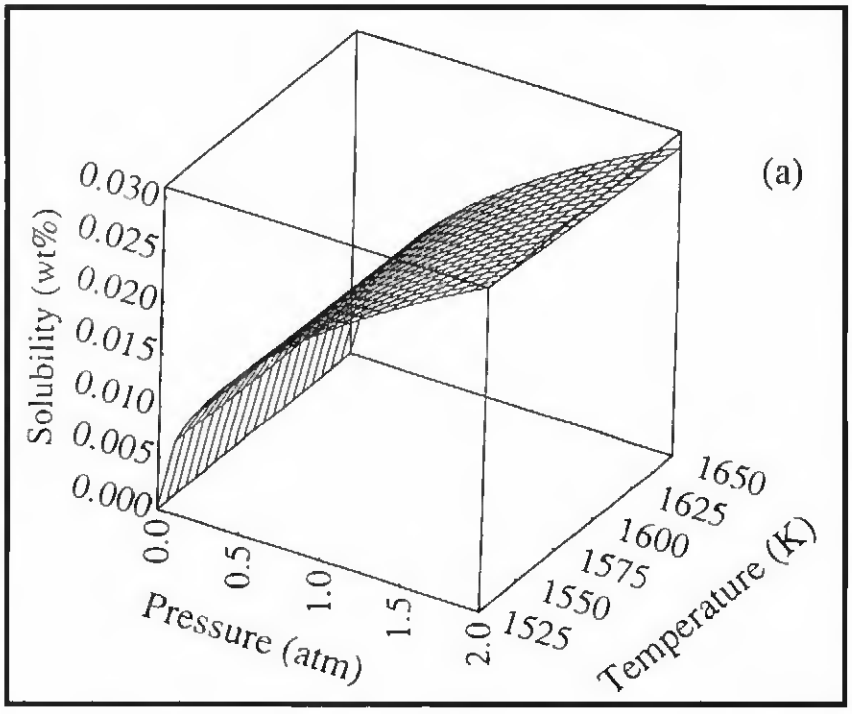

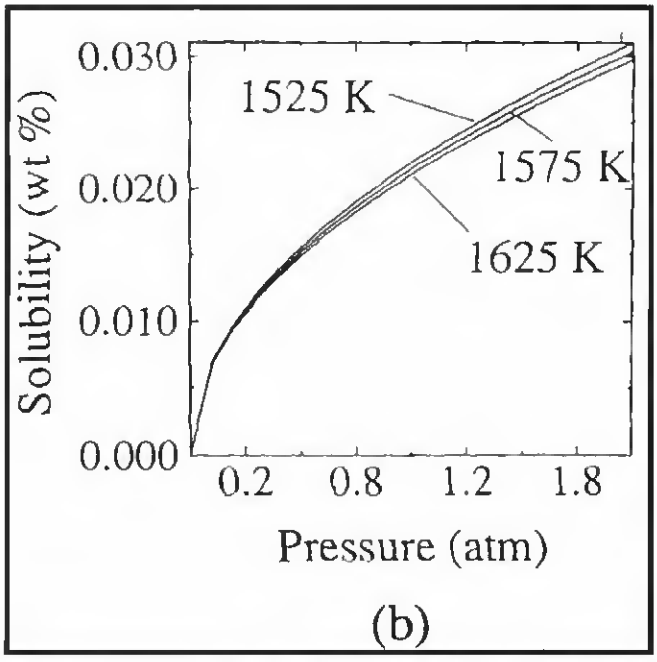

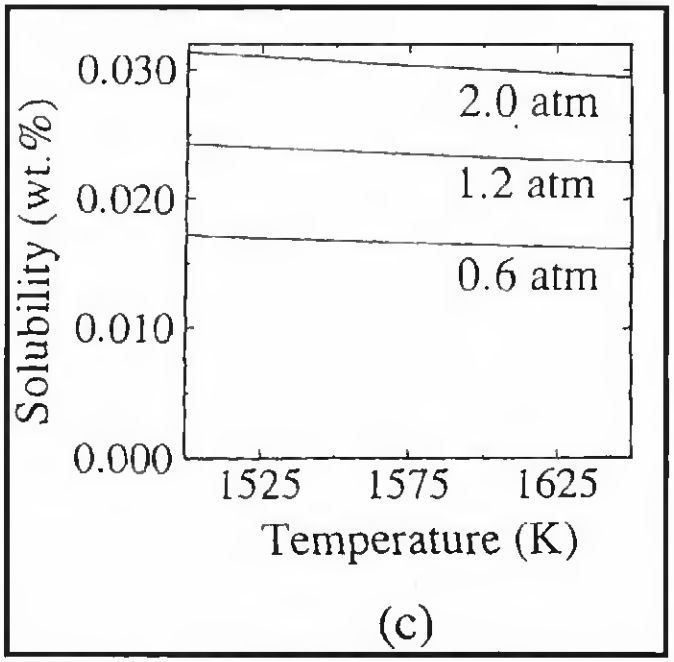

Fig. 3 — Computed equilibrium solubility of nitrogen in iron exposed to diatomic nitrogen. A — as a function of temperature and partial pressure of diatomic nitrogen; B — as a function of partial pressure of diatomic nitrogen at three temperatures; C — as a function of temperature at three partial pressures of diatomic nitrogen.

enhanced dissolution of nitrogen in the weld metal. Atomic and excited gases and electrons present in the gas phase introduce several special features to the system. Of these, three issues are of special interest in welding: the extent of dissociation of a diatomic gas in the welding environment; the effect of temperature on the species concentration in the weld metal for different gases; and the concentration of dissolved species in the weld pool retained by the weld metal after cooling.

Welding is a complex operation in which a large number of physical processes occur simultaneously, each affecting the other. In order to understand any single one of these processes, it is necessary to isolate this process from the others and study it individually. Physical modeling experiments allow for the individual process to be studied with much greater ease than attempting to control an actual welding process to achieve the same results. In the physical modeling experiments undertaken here, the partitioning of nitrogen between the weld metal and its plasma environment is considered. Small high-purity iron samples are used to avoid the problems of interaction of alloying elements and spatial variations of temperature across the surface of the sample. In addition, the weld metal-plasma interaction is studied with the aid of a glow discharge plasma. A comparison between several major features of the plasmas created by both arc welding and laser/electron beam welding and those of glow discharge plasmas is presented in Table 1. It is observed that the species present in the welding plasmas, *e.g.*, electrons, ions, excited neutral atoms and molecules, and monatomic and diatomic species, can be created in glow discharge plasmas. Furthermore, typical electron energies in a glow discharge plasma are comparable with that commonly present during high energy density beam or arc welding processes. Typical electron densities in glow discharge plasmas are somewhat lower than those in plasmas created during arc welding and laser/electron beam welding processes. For the purpose of physi-

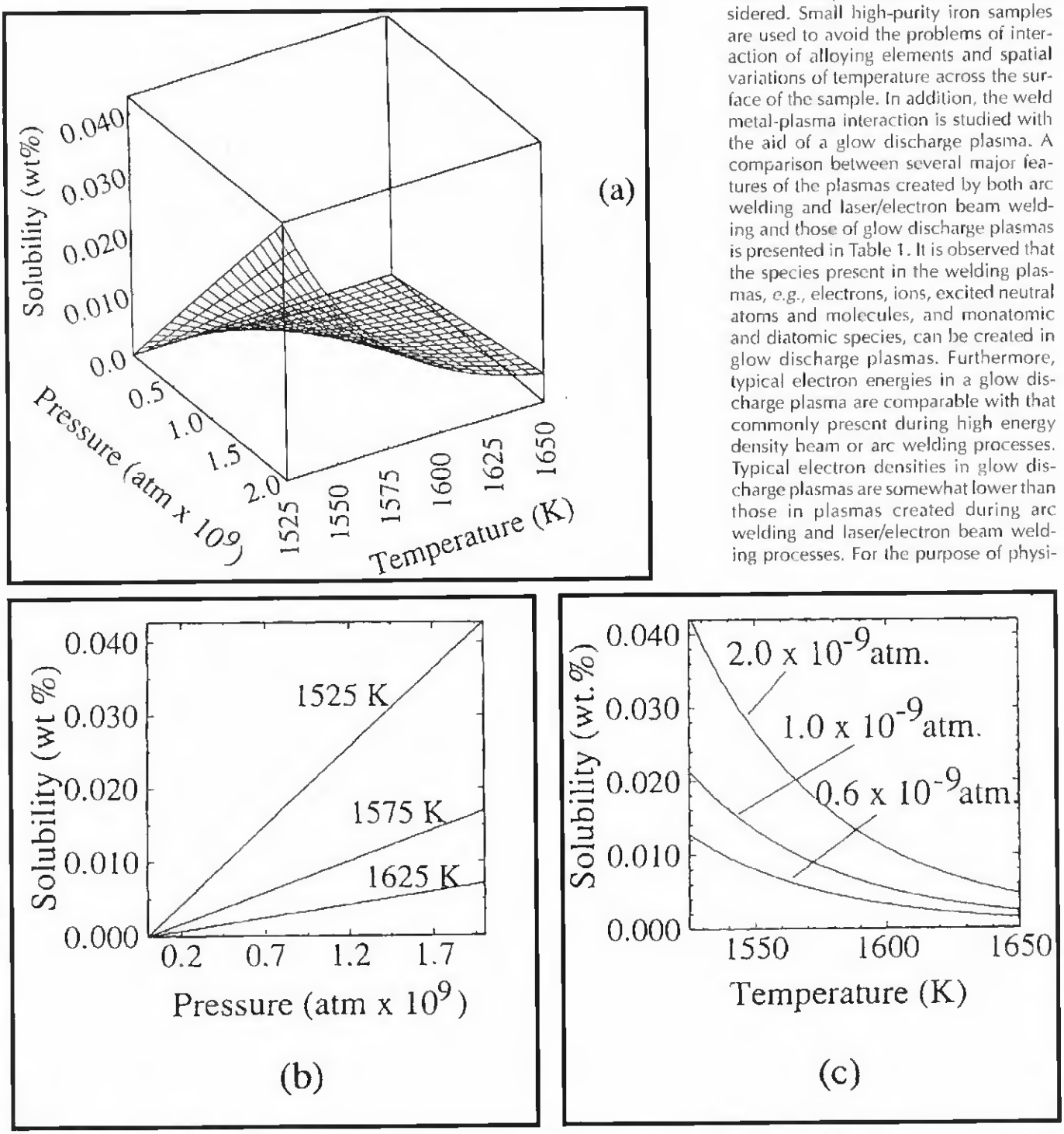

Fig. 4 — Computed equilibrium solubility of nitrogen in iron exposed to monatomic nitrogen. A — As a function of temperature and partial pressure of monatomic nitrogen; B — as a function of partial pressure of monatomic nitrogen at three temperatures; C — as a function of temperature at three partial pressures of monatomic nitrogen.

cal simulation, glow discharge plasmas are attractive since they can be generated at low energy density and their use does not lead to temperature gradients on the sample surface. On the whole, the glow discharge provides an appropriate method for simulating the plasma present above the weld metal for the study of the partitioning of nitrogen.

The research reported in this paper is aimed at achieving an improved understanding of the enhanced solubility of nitrogen in the weld pool through physical modeling. Experiments were conducted under isothermal conditions in which small iron samples were exposed to a well-characterized plasma, quenched, and the nitrogen contents determined. A quantitative analysis of the data from the nitrogen dissolution experiments was performed to better understand the relation between the enhanced solubility and the processing conditions. The enhanced solubility could be explained on the basis of a model that considered homogeneous dissociation of the diatomic gas in the presence of an energy source and the dissolution of nitrogen at the temperature of the metal surface.

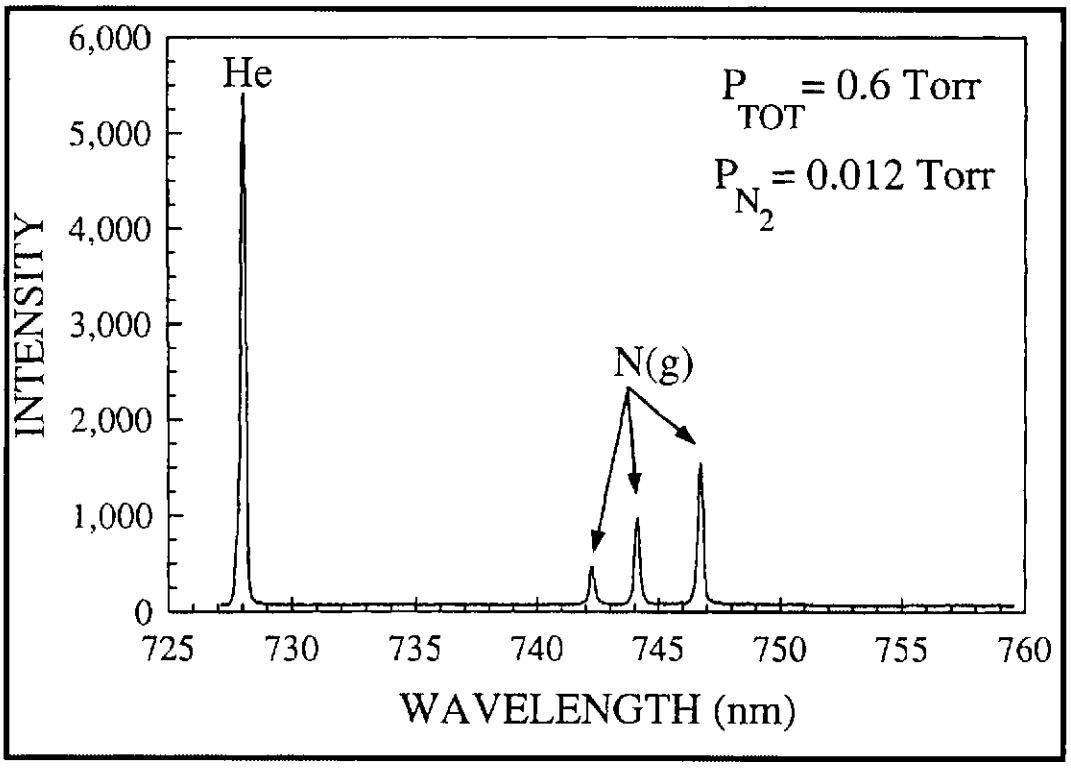

Fig. 5 — A typical intensity vs. wavelength plot for a He-2%N_2 plasma.

Table 3 — Experimentally Determined Concentration of Nitrogen in Solid Iron at 1573 K Exposed to Controlled Nitrogen Plasmas Composed of a Feed Gas Composition of 100% for a Period of 45 Minutes

Total Pressure (atm.)	Sieverts' Law Approximation (ppm)	Nitrogen Concentration (ppm)	P_N (atm.) due to Thermal Dissociation	P_N (atm.) due to Plasma
7.89×10^{-4}	6.04	97	6.9×10^{-11}	1.11×10^{-9}
7.89×10^{-4}	6.04	151	6.9×10^{-11}	1.73×10^{-9}
1.053×10^{-3}	6.98	195	7.97×10^{-11}	2.23×10^{-9}
1.053×10^{-3}	6.98	155	7.97×10^{-11}	1.77×10^{-9}
1.316×10^{-3}	7.8	106	8.91×10^{-11}	1.21×10^{-9}
1.316×10^{-3}	7.8	90	8.91×10^{-11}	1.03×10^{-9}
1.579×10^{-3}	8.54	145	9.76×10^{-11}	1.66×10^{-9}
1.579×10^{-3}	8.54	45	9.76×10^{-11}	5.14×10^{-10}

Table 4 — Data Used in the Calculation of Electron Density

Constants	Symbol	Value
Rest Mass of Electron	m_e	9.1095×10^{-31} kg
Boltzmann Constant	k	1.38066×10^{-23} J/K
Electron Temperature	T	5000 K
Plancks Constant	h	6.62662×10^{-34} J-sec
Ionization Potential	V	2.3277×10^{-18} J
Partition Function of an Electron	Z_e	2

Table 5 — Data Used in the Calculation of Partition Functions

Degeneracy, g_i, (Ion)	Energy Level (Ion) (cm^{-1})	Degeneracy, g_i, (Atom)	Energy Level (Atom) (cm^{-1})
1	0	4	0
3	48.7	6	19224.5
5	130.8	4	19233.2
5	15316.2	2	28838.9
1	32688.8	4	28839.3

Experimental

Figure 1 is a schematic diagram of the experimental setup, which can be divided into three main parts: the radio frequency (RF) generator, the reaction chamber, and the emission spectroscopy equipment. A 10-kW RF generator with a frequency of 450 kHz was utilized to create inductively coupled RF plasmas from the feed gases. The RF energy was applied through a copper coil wound around a quartz reaction tube with an outer diameter of 48 mm. A photograph of a representative glow-discharge plasma created in this experimental setup is shown in Fig. 2.

An iron disc, 5 mm in diameter and 1.5 ±0.2 mm in thickness, was placed in the reaction chamber within the area defined by the copper coils by the use of a tantalum wire specimen holder, which

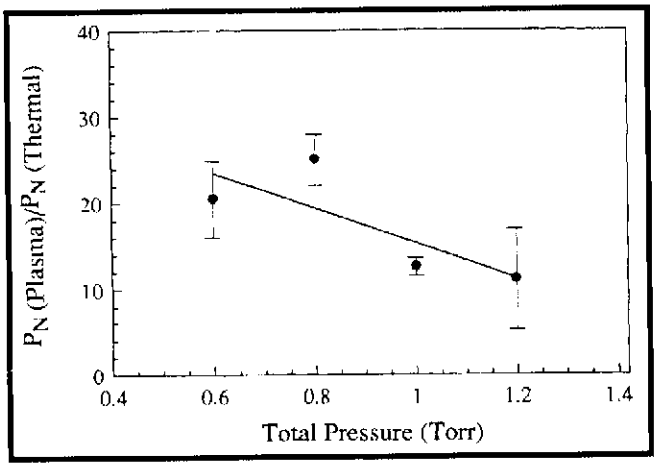

Fig. 6 — Relationship between the ratio of the computed monatomic nitrogen partial pressure in the plasma based on the experimental nitrogen solubility and the monatomic nitrogen partial pressure owing to thermal dissociation of $N_2(g)$ and the total pressure in the experimental chamber.

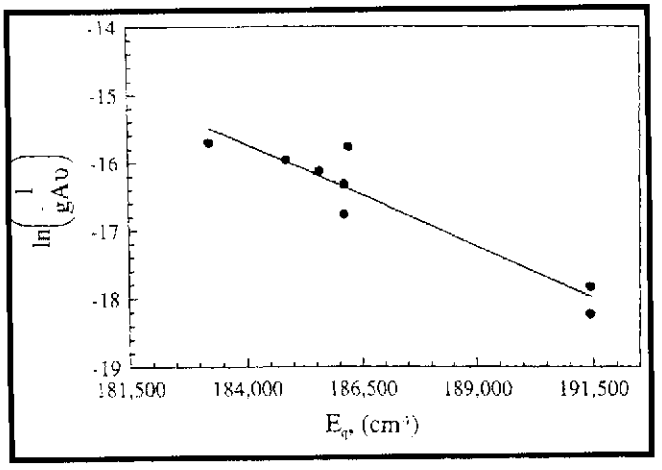

Fig. 7 — Typical Boltzmann plot for a pure helium plasma at 1.2 Torr total pressure used to calculate electron temperature.

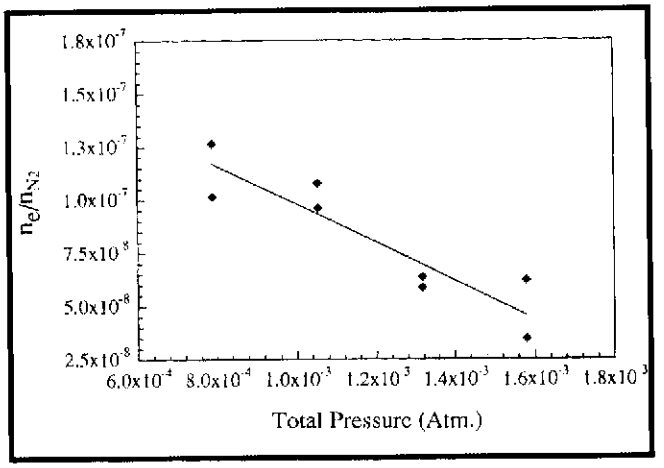

Fig. 8 — Plot of the ratio of electron density and atomic density vs. the total pressure for an electron temperature of 5000 K.

minimized the contact area between the sample and the holder. Sample temperature, measured through the use of a two-color optical pyrometer, was maintained at 1573 K ±20 K for a period of 45 minutes. This temperature falls in the austenite region of the Fe-C phase diagram, and, therefore, the Fe sample remains in the solid state. The nitrogen pickup in the solid sample is different from that observed in a molten metal. However, our goal was to focus on the principles of partition of nitrogen between a plasma and a metal. It was not our goal to determine the absolute value of nitrogen concentration in the weld pool. Sample temperatures were maintained by manipulating the power input from the RF generator. A pure nitrogen atmosphere was created in the reaction chamber by introducing ultra-high-purity nitrogen at a flow rate of 100 SCCM. Total pressures for the experiments were maintained between 0.6 and 1.2 Torr. After exposing the samples to a plasma for a predetermined time, the samples were quenched inside the experimental chamber by turning off power to the generator and allowing gas to flow over the sample. The nitrogen concentration in the samples was determined from vacuum fusion analysis.

Spectroscopic data were gathered using an EG&G Princeton Applied Research Corporation (PARC) model 1235 Digital Triple Grating Spectrograph connected to a Model 1430-P Charge Coupled Device (CCD) Detector. This setup was controlled by a 386 personal computer using an optical multichannel analyzer applications software package (EG&G PARC OMA SPEC 2000). Throughout all of the spectroscopic analyses, a 1200 gratings/mm diffraction grating was used. Optical emissions from the plasmas could be analyzed from both the top and the side of the setup through the use of a fiber-optic cable connected to the CCD detector.

Results and Discussion

Thermodynamics of Nitrogen Dissolution in Iron

The computed equilibrium concentration of nitrogen in iron, based on Sieverts' Law, is shown in Fig. 3A–C. The standard free energy data (Refs. 10–11) used in the calculations are presented in Table 2. The calculated values show that at a given partial pressure of diatomic nitrogen, the equilibrium nitrogen concentration decreases slightly with temperature. On the other hand, the equilibrium concentration increases linearly with the square root of the partial pressure of diatomic nitrogen at a given temperature. The effects of temperature and partial pressure are illustrated more fully in Fig. 3B and C, respectively, in two-dimensional sections of the data presented in Fig. 3A. Figure 3C shows that the solubility of diatomic nitrogen species in γ-Fe decreases only a small amount over the temperature range of interest for a number of nitrogen partial pressures. Similarly, the computed equilibrium solubility of monatomic nitrogen gas in solid iron is shown in Fig. 4A–C and is based on the free energy data in Table 2 and Equations 10 and 11.

$$N(g) \rightarrow \underline{N}(wt\ \%) \qquad (10)$$

$$\underline{N}(wt\ \%) P_N e^{-\frac{\Delta G^{o}_{10}}{RT}} \qquad (11)$$

In contrast to the iron-diatomic nitrogen system, the iron-monatomic nitrogen equilibrium system displays much different behavior. The equilibrium solubility of nitrogen in iron exposed to monatomic nitrogen increases in a linear manner with respect to increasing monatomic nitrogen partial pressure, as shown in Fig.

Table 6 — Calculated Number Densities of Electrons, Atoms and Molecules

Total Pressure (Atm.)	P_N (Plasma) (Atm.)	Electron Density, n_e (m^{-3})	Number Density of Nitrogen Atoms (m^{-3})	Number Density of Nitrogen Molecules (m^{-3})
7.89×10^{-4}	1.11×10^{-9}	1.175×10^{14}	1.630×10^{15}	1.159×10^{21}
7.89×10^{-4}	1.73×10^{-9}	1.467×10^{14}	2.540×10^{15}	1.159×10^{21}
1.053×10^{-3}	2.23×10^{-9}	1.665×10^{14}	3.274×10^{15}	1.545×10^{21}
1.053×10^{-3}	1.77×10^{-9}	1.483×10^{14}	2.599×10^{15}	1.545×10^{21}
1.316×10^{-3}	1.21×10^{-9}	1.227×10^{14}	1.776×10^{15}	1.932×10^{21}
1.316×10^{-3}	1.03×10^{-9}	1.132×10^{14}	1.512×10^{15}	1.932×10^{21}
1.579×10^{-3}	1.66×10^{-9}	1.437×10^{14}	2.437×10^{15}	2.318×10^{21}
1.579×10^{-3}	5.14×10^{-9}	7.994×10^{13}	7.546×10^{14}	2.318×10^{21}

4B, and decreases significantly in a nonlinear manner according to temperature over the defined range of temperatures, as shown in Fig. 4C. Since the monatomic nitrogen solubility increases rather sharply with decreasing temperature below 1575 K, small changes in temperature can cause large changes in the ensuing equilibrium nitrogen concentration. When compared, this variation in temperature plays a much greater role than that of pressure in determining the extent of nitrogen solubility in iron exposed to monatomic nitrogen gas.

In the plasma, the concentration of atomic nitrogen gas, which is formed from diatomic nitrogen, is higher than what would be obtained solely from the consideration of thermal equilibrium between these two species at the system temperature and pressure. If the actual concentration of the atomic nitrogen were known, its concentration in iron could be estimated considering equilibrium between the atomic nitrogen and the metal. In the plasma, the extent of dissociation of diatomic nitrogen depends on factors such as the nature of the power source, the energy dissipated, the overall system geometry, and the nature of the diatomic gas. We define a hypothetical temperature, T_d, at which the equilibrium thermal dissociation of the diatomic nitrogen would produce the actual partial pressure of monatomic nitrogen present in the plasma. The partial pressure of the monatomic nitrogen in the plasma is given by:

$$P_N = \left\{P_{N_2}\right\}^{\frac{1}{2}} e^{-\frac{\Delta G^{\circ}_{13}\big|_{T_d}}{RT_d}} \tag{12}$$

where P_{N2} is the partial pressure of diatomic nitrogen in the plasma and ΔG°_{13} is the standard free energy for reaction 13.

$$\frac{1}{2}N_2(g) \rightarrow N(g) \tag{13}$$

The extent of dissociation of diatomic nitrogen at T_d can be calculated from Equation 12. Since the extent of dissociation of diatomic nitrogen is low under typical welding conditions and in glow discharge plasmas, P_{N_2} can be assumed to be equal to the partial pressure of N_2 in the inlet gas, $P^{in}_{N_2}$. Combining Equations 11 and 12, and remembering that the dissociation of $N_2(g)$ is considered at T_d and the dissolution of N(g) at T_s we get the equilibrium nitrogen concentration in iron.

$$\underline{N}(wt\ \%) = \sqrt{P^{in}_{N_2}}\, e^{-\frac{1}{R}\left(\frac{\Delta G^{\circ}_{13}}{T_d} + \frac{\Delta G^{in}_{16}}{T_s}\right)} \tag{14}$$

Equation 14 indicates the solubility of nitrogen in iron exposed to a plasma environment with the sample at a temperature T_s. The hypothetical dissociation temperature, T_d is higher than the temperature of the sample, T_s, and is a measure of the partial pressure of the atomic nitrogen in the plasma. For the experimental conditions in this study, the magnitude of T_d is calculated by inserting the experimental solubility into Equation 14 and solving this equation for T_d.

If a system consisting of monatomic and diatomic nitrogen and iron is in equilibrium, the nitrogen solubility in iron can be readily calculated considering equilibrium between the iron and either the diatomic or monatomic forms of nitrogen. Let us consider such a system at 2000 K and 1 atm total pressure. At equilibrium, the gas will consist of 0.99999909 atm of $N_2(g)$ and 9.1×10^{-7} atm of N(g). The equilibrium nitrogen solubility considering equilibrium between diatomic nitrogen gas at 0.99999909 atm and 2000 K and iron is 0.0045 wt-% N. The equilibrium nitrogen solubility in iron exposed to monatomic nitrogen gas at 2000 K and a partial pressure of 9.1×10^{-7} atm is also 0.0045 wt-% N.

In the scheme of calculations considered in this paper, the monatomic nitrogen gas is not in equilibrium with the diatomic gas at the temperature of the iron sample. In that respect, there is some difference between the straightforward preceding example and the complex welding problem. Gedeon and Eagar (Ref. 9) have considered equilibrium between iron and diatomic and monatomic hydrogen and assume that the overall solubility is the sum of solubilities of diatomic hydrogen/iron and monatomic hydrogen/iron systems. In the nitrogen system of interest in this paper, the concentration of dissolved nitrogen in iron in equilibrium with monatomic gas is significantly higher than the nitrogen concentration in equilibrium with diatomic nitrogen gas. This is because the partial pressure of monatomic nitrogen gas is far in excess of what is expected under equilibrium conditions as a result of thermal dissociation of diatomic nitrogen. For the conditions described in this paper, the contribution of diatomic nitrogen gas is insignificant in the calculation of the nitrogen concentration in the metal. Its primary role is to act as a precursor for the generation of monatomic species at a partial pressure which is far in excess of the amount expected from thermal dissociation at the temperature of the sample because of the presence of a plasma phase.

Table 7 — Computed Dissociation Temperatures for Various Experiments. Sample Temperature was 1573 K

Total Pressure (atm.)	Experimental Solubility (ppm)	Dissociation Temperature, T_d (K)
1.579×10^{-3}	45	1673
1.579×10^{-3}	145	1752
1.316×10^{-3}	106	1737
1.316×10^{-3}	90	1725
1.053×10^{-3}	195	1788
1.053×10^{-3}	155	1771
7.89×10^{-4}	97	1748
7.89×10^{-4}	151	1780

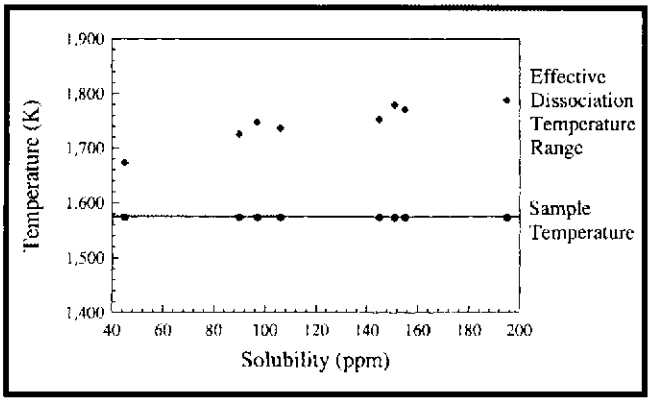

Fig. 9 — Comparison of the nitrogen solubility (wt-%) and the effective dissociation temperature over the experimental pressure range.

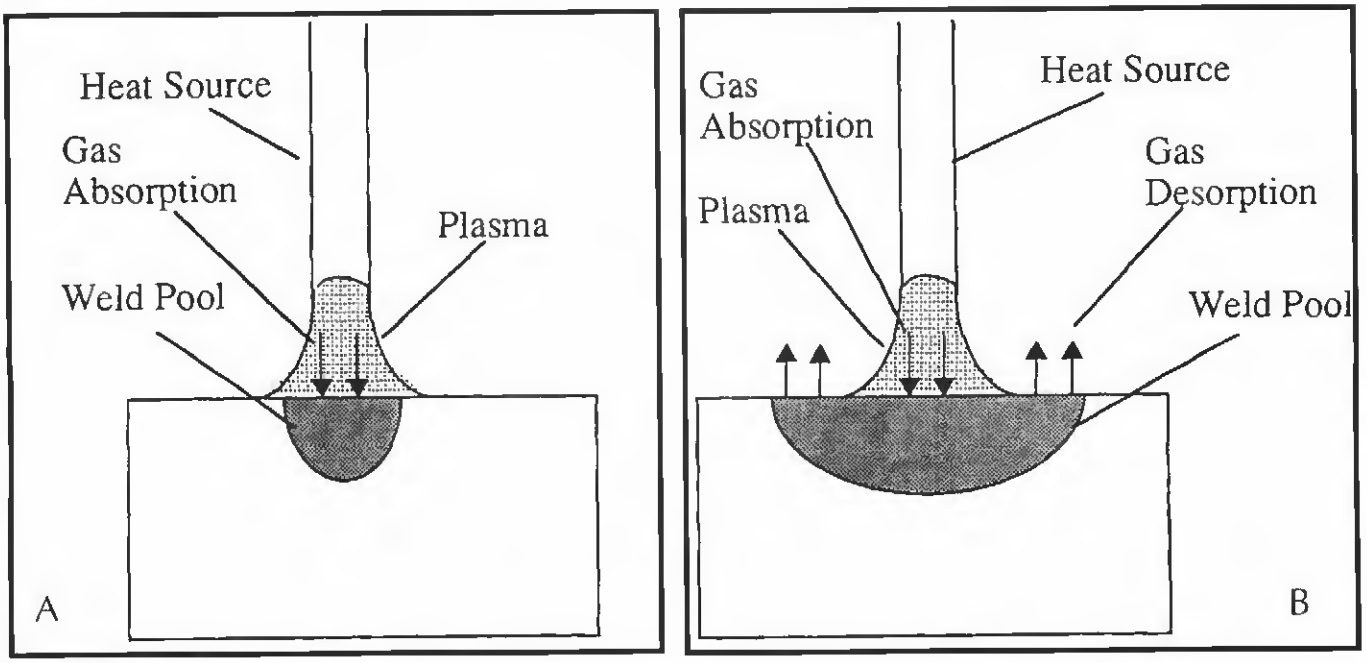

Fig. 10 — Schematic diagrams of a weld pool. A — completely covered by a plasma; B — incompletely covered by a plasma.

Analysis of Experimental Data

Measured nitrogen solubilities as a function of reactor pressure at a constant sample temperature (1573 K) are presented in Table 3. The data show that the nitrogen concentration in each case is significantly higher than that expected from calculations based on Sieverts' law. Previous researchers found that when a metal is exposed to a plasma formed from a diatomic source gas, the gas solubility values are significantly higher than the Sieverts' Law predictions. This enhanced solubility has been attributed to monatomic gaseous species in the plasma, and the presence of monatomic nitrogen in our experimental plasmas has been confirmed by optical emission spectroscopy. A typical intensity vs. wavelength plot for a He-2%N_2 plasma is shown in Fig. 5, where prominent atomic nitrogen peaks at 742.36, 744.23, and 746.83 nm are clearly visible. On the other hand, in the range of wavelengths analyzed spectroscopically, no diatomic nitrogen peaks were observed.

The atomic nitrogen partial pressures in the plasma can be estimated from the experimental values of nitrogen concentrations in the iron samples and the sample temperature using Equation 11. The computed values of atomic nitrogen partial pressures for all the experiments along with the partial pressures of atomic nitrogen in thermal equilibrium with diatomic nitrogen for the sample temperature and the feed gas nitrogen partial pressure are presented in Table 3. The atomic nitrogen partial pressures in the plasma should be higher than those produced solely by equilibrium thermal dissociation of diatomic nitrogen gas at the experimental conditions. A higher partial pressure of monatomic nitrogen in the plasma over that of thermal dissociation of diatomic nitrogen molecules is observed owing to the additional effects of electrical induction produced by the power source and collisional processes characteristic of a plasma.

The calculated ratios of the monatomic nitrogen partial pressures in the plasma and the equilibrium partial pressures of monatomic nitrogen owing to thermal dissociation of $N_2(g)$ at the sample temperature are plotted as a function of total pressure in Fig. 6. There is a measure of scatter in the data plotted in Fig. 6, which can be traced back to the steep temperature dependence of the equilibrium solubility of monatomic nitrogen as shown in Fig. 4. In this relationship, a small change in temperature can cause a pronounced change in the equilibrium nitrogen concentration. Since the monatomic nitrogen partial pressures in the plasma are computed directly from the nitrogen concentration in the samples, this effect is carried over into Fig. 6. The data, nevertheless, show a trend in which the ratio decreases with an increase in total pressure, which is consistent with the increased importance of collisional processes at low pressures. The generation of monatomic nitrogen gas in the plasma involves the collision of diatomic nitrogen molecules with fast electrons (Ref. 6). Therefore, to understand the variation of atomic nitrogen partial pressure in the plasma with pressure, it is necessary to examine how the electron density varies with the total pressure. The number density of electrons was calculated for different total pressures. The calculation is based on the reaction of an atom forming an ion and an electron, *i.e.*, $N(g) \rightarrow N^+ + e^-$, and is formalized by Saha's equation (Ref. 12).

$$\frac{n_e n_i}{n_N} = \frac{Z_e Z_i \left(2\pi m_e kT\right)^{\frac{3}{2}} e^{\left(\frac{-V}{kT}\right)}}{Z_n h^3} \qquad (15)$$

where n_e, n_i, and n_N are the particle number densities of electrons, ions, and neutral atoms, respectively. T is the absolute temperature, and V is the ionization potential, while m_e is the rest mass of an electron. k is the Boltzmann's constant, and h is the Planck's constant. The internal partition functions, Z_e Z_i and Z_N, are defined by the following equation

$$Z = \sum_j g_j e^{\frac{-u_j}{kT}} \qquad (16)$$

where g_j is the degeneracy or statistical weight corresponding to the energy level, u_j. The following equation is for a monatomic gas:

$$g = 2S + 1 \qquad (17)$$

in which S is the vector sum of the spin numbers. The partition functions were calculated from the data given in the National Bureau of Standards' (NBS) *Tables of Atomic Energy Levels* compiled by Moore (Ref. 13), and the degeneracy of

electrons is taken to be equal to two. Quasi-neutrality of charge and ideal gas behavior, represented in Equations 18 and 19, are assumptions used in the calculation of the number densities along with the assumption of kinetic equilibrium ($T_e = T_i = T_N = T$).

$$n_e = n_i \tag{18}$$

$$n_N = \frac{N_A}{V_m} \times \frac{273}{T} \times P_N \tag{19}$$

where N_A is Avagadro's number (6.023×10^{23}), V_m is the volume occupied by one mole of gas at standard temperature and pressure (22.4×10^{-3} m^3/mol), P_N is the pressure of atomic nitrogen, and T is the temperature. Thus, the values of the population density of the electrons, (n_e), ions, (n_i), and atomic nitrogen, (n_N), can be determined from Equations 15, 16, and 19 if the electron temperature, T, is known.

The electron temperature was determined from spectral data taken from He-N_2 plasmas. Because of the dominant effect of the molecular spectra over the atomic nitrogen peaks in pure nitrogen plasmas, helium plasmas containing a trace amount of nitrogen were analyzed. The following equation, based on the assumptions that electron energies follow a Boltzmann distribution and local thermal equilibrium is attained, was used.

$$ln\left(\frac{I}{gAv}\right) = lnC - \left(\frac{E_q}{kT}\right) \tag{20}$$

where I is the integrated intensity, g is the degeneracy of the upper energy level q, A is the transition probability for the transition from state q to the lower energy level, V is the frequency, E_q is the energy associated with the level q, k is the Boltzmann constant, T is the electron temperature, and C is a constant. The electron temperature is then obtained from a plot of the left-hand side of Equation 20 vs. E_q. A typical plot is shown in Fig. 7. The electron temperatures for the plasmas formed from various He-N_2 mixtures and total pressures fell within a range of temperatures from approximately 4880 K at 0.6 Torr total pressure to 4680 K at 1.2 Torr total pressure for plasmas composed of an inlet gas of He-2%N_2. This range of electron temperature is somewhat higher than the 3400 to 4200 K electron temperatures reported by Peebles and Williamson (Ref. 14) for the Nd:YAG laser assisted welding of commercial 1100 aluminum alloy. The values are comparable to the 5050 K electron temperature for Cr I lines reported by Shaw (Ref. 15) and somewhat lower than the values reported by Collur and DebRoy (Ref. 16) and Miller and DebRoy (Ref. 17) both for CO_2 laser welding of stainless steels. Thus, the observed electron temperatures are well within the range of electron temperatures reported in the literature.

Using an average electron temperature of 5000 K, the electron densities were calculated for different partial pressures of atomic nitrogen in the plasma from Equations 11, 18, and 19. The data used in these calculations are presented in Tables 4 and 5, and the computed electron density values are presented in Table 6. The values for the electron densities are consistent with the values common in process plasmas, (Ref. 18) and the number density of electrons decreases with increase in total pressure. A plot of the ratio of the number density of electrons to that of the nitrogen molecules as a function of total pressure is plotted in Fig. 8. This plot shows that this ratio decreases with increasing total pressure, indicating again, the importance of collisional processes at low pressures and the facilitation of these processes at these pressures. The results are also consistent with the mechanism of formation of nitrogen atoms in the plasma. It has been pointed out that the formation of atomic nitrogen is a consequence of the collision of fast electrons with the nitrogen molecules (Ref. 19). Since the average electron energy of the plasma is relatively insensitive to the total pressure in the range of pressures investigated in this work, the formation of atomic nitrogen depends on the electron density. Since the electron density decreases with increase in pressure, as observed from Fig. 8, the partial pressure of atomic nitrogen also decreases with pressure.

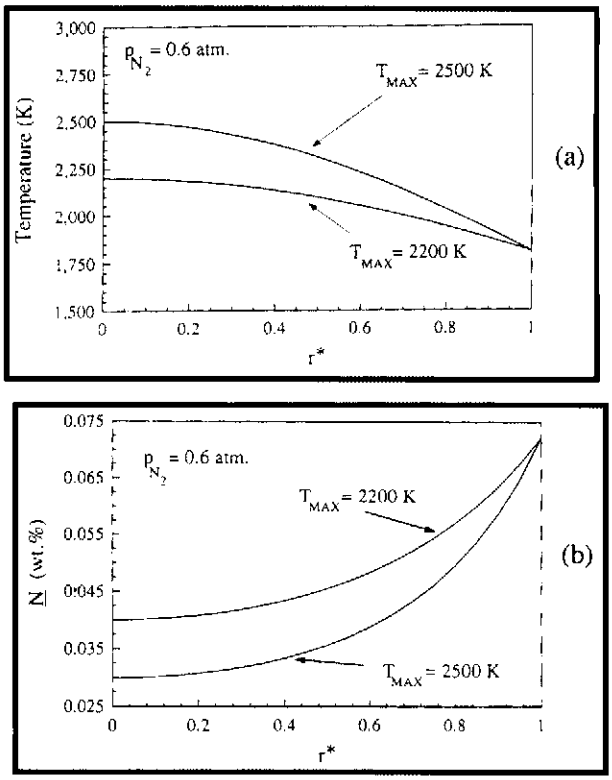

Fig. 11 — Computed values for: A — temperature; B — nitrogen concentration across the radius of the weld pool for T_{MAX} values of 2500 K and 2200 K and diatomic nitrogen partial pressure of 0.6 atm.

The observed high concentrations of nitrogen in iron can be explained by assuming that the atomic nitrogen partial pressure in the plasma can be effectively modeled by a hypothetical thermal dissociation of diatomic nitrogen at a temperature higher than the sample temperature and represented as T_d. At this temperature, thermal dissociation of N_2 produces a partial pressure of atomic nitrogen gas equal to that in the plasma. For each experiment, the effective dissociation temperatures can be calculated from the measured values of the nitrogen concentration in iron, partial pressure of diatomic nitrogen in the feed gas, and the sample temperature using Equation 14. The computed dissociation temperatures are plotted in Fig. 9 as a function of the total pressure and are presented in Table 7. The calculated dissociation temperatures for all of the experimental solubility values are approximately 100 to 215 K higher than the sample temperature. These values agree well with the results obtained from the analysis of several independent experimental data sets from plasma-metal systems reported recently (Ref. 20). The results reported there (Ref. 20) are consistent with our previous observation that if experimental data are not available, a rough estimate of the nitrogen concentration may be obtained by assuming a hypothetical dissociation temperature about 100 to 200 K higher than the sample temperature.

Application to Welding

Kuwana and Kokawa (Ref. 21) investigated the gas tungsten arc (GTA) welding of a low-alloy steel in controlled nitrogen environments. They measured nitrogen concentration in the weld pool for various welding conditions. Here, we examined the application of the results of

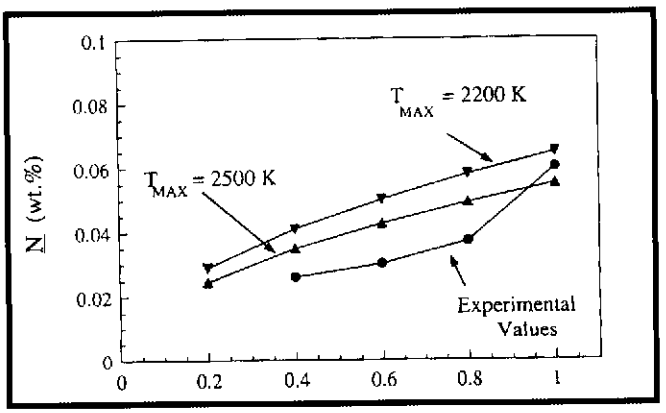

Fig. 12 — Comparison between the experimental nitrogen solubility results of Kuwana and Kokawa (Ref. 21) and the computed nitrogen solubility predictions based on the physical modeling experiments.

the physical modeling experiments to the actual welding experiments performed by these investigators (Ref. 21).

Unlike the physical modeling experiments reported in this paper, the temperature of the weld pool surface during the welding operation shows a significant spatial variation. If the partial pressure of diatomic nitrogen was the main factor in determining the nitrogen concentration in the weld metal, the consequences of the spatial variation in the weld pool surface temperature would he rather unimportant. This fact can be appreciated from Fig. 3, in which the equilibrium nitrogen concentration is observed to be insensitive to variations in temperature. In contrast, for monatomic nitrogen species, a slight variation in the temperature can lead to a significant variation in the equilibrium solubility of nitrogen as shown in Fig. 4. Indeed, for this system, the equilihrium nitrogen concentration increases significantly with a small decrease in temperature. Rigorous calculation of the nitrogen concentrations in the weld pool from hasic principles is very complex and beyond the scope of this paper. However, it is shown that by making a few simplifying assumptions, the results of the physical modeling experiments can be utilized to understand the results of actual welding experiments (Ref. 21).

First, the extent of coverage of the weld pool by the plasma, as shown in Fig. 10A and B, is determined by welding variables. In the welding data examined here, a fairly small weld pool approximately 4 mm wide was formed and an arc current of 250 A was used. Thus, complete coverage of the weld pool by the plasma, as shown in Figure 10A, is assumed. Second, to compare their experimental data with calculations, it is necessary to know the temperature distribution at the surface of the weld pool, which is not known for these experimental conditions. Khan (Ref. 22) has shown that the temperature distribution at the surface of the weld pool can be represented by Equation 21.

$$T = T_{MAX}\, e^{-ar^{*2}} \qquad (21)$$

where T is the temperature at any location, T_{MAX} is the weld pool surface temperature at the axis of the arc, a is a constant, and r* is the dimensionless distance from the axis of the arc given by the ratio, r/r_o. In this ratio, r is the radial distance from the center of the molten pool or axis of the arc, and r_o is the radius of the molten pool. Since the temperature at the solid/liquid interface, *i.e.*, at $r = r_o$, is known, the value of the variahle a can be calculated if the value of T_{MAX} is known. Figure 11A shows two temperature profiles for two assumed values of T_{MAX}.

Third, apart from the surface temperature distribution, the values of the dissociation temperature are necessary to calculate the nitrogen concentration distribution of the weld pool surface from Equation 14. The value of the dissociation temperature, T_d, is higher than the surface temperature. The exact difference between the surface temperature and the dissociation temperature depends on the concentration of atomic nitrogen gas in the plasma, which, in turn, depends on the properties of the plasma, such as the electron temperature and electron density. In the physical modeling experiments, the dissociation temperatures were found to be about 100 to 200 K higher than the sample temperature. These results are interpreted as showing that the higher the computed effective dissociation temperature, the higher the atomic nitrogen gas partial pressure in the plasma. In view of the large welding velocity (1.67 mm/s) in the experiments of Kuwana and Kokawa (Ref. 21), it is believed that the plasma continually mixes with the surrounding gas and a small difference between the dissociation temperature and the surface temperature of the weld pool is appropriate. A temperature difference of 125 K between the dissociation temperature and the surface temperature is assumed based on the final nitrogen concentrations reported (Ref. 21).

The equilibrium concentration of nitrogen at all locations on the surface of the weld pool can be computed from Equation 14 once the dissociation temperature at each of these locations is known. The computed values of nitrogen concentration are shown as a function of dimensionless distance in Fig. 11B. The nitrogen concentrations are higher at the outer edge of the weld pool since the monatomic nitrogen solubility increases rather sharply with decreasing temperature. This phenomenon has also been postulated (Ref. 9) in the enhanced dissolution of hydrogen. In view of the fact that the liquid metal in the weld pool undergoes vigorous recirculation (Ref. 23, 24), the nitrogen from the surface is readily transported to the interior of the weld pool.

Finally, we assume that the overall nitrogen concentration of the weld metal, $(\text{wt-}\%\underline{N})_{av}$, if the nitrogen is not lost from the pool in any appreciahle amount, is determined by an average concentration of nitrogen on the weld pool surface integrated over the entire surface

$$(wt\ \%\underline{N})_{av} = \frac{1}{\pi r_o^2}\int_0^{r_o} 2\pi r\,[wt\ \%\underline{N}]dr = \int_0^1 2r^*\,[wt\ \%\underline{N}]dr^* \qquad (22)$$

where [wt-%N] is the local value of nitrogen concentration at any location on the weld pool surface and r^* (= r/r_o) is the dimensionless radial distance from the axis of the heat source on the weld pool surface.

The computed overall concentration of nitrogen in the weld pool is shown in Fig. 12 as a function of P_{N2} in H_2-N_2 mixtures from the experimental data of Kuwana and Kokawa (Ref. 21) for two values of T_{MAX}. The calculations show that a fair agreement is reached between the computed results and the experimental data. An improved agreement between the experimental data and the predicted values can be obtained by selecting a temperature difference of about 100 K between the surface temperatures and the dissociation temperatures. However, the calculations demonstrate that the findings of the physical modeling experiments can be applied to understanding dissolution of nitrogen in

the weld metal.

Summary and Conclusions

Physical modeling experiments were performed to provide an understanding of the partitioning of nitrogen between the weld metal and its plasma environment. Small high-purity iron samples maintained at a constant temperature were exposed to low pressure nitrogen plasmas and analyzed for the resulting nitrogen contents. The nitrogen concentrations in each case were significantly higher, up to 30 times, than that predicted by equilibrium calculations using Sieverts' law. The results were consistent with the presence of atomic nitrogen gas in the plasma at a partial pressure that is significantly in excess of that anticipated from thermal equilibrium between the diatomic and the atomic nitrogen species at the temperature of the sample. This higher-than-equilibrium partial pressure of atomic nitrogen gas in the plasma was modeled by an equivalent thermal dissociation of diatomic nitrogen at a dissociation temperature higher than the sample temperature. In each case, the dissociation temperature was found to be between 100 and 210 K higher than the sample temperature. The results were applied to actual GTA welding experiments previously reported in the literature in order to explain the nitrogen solubility results. The observed nitrogen concentrations in the pure iron weld metals could be explained by the calculation of atomic nitrogen partial pressure profiles on the weld pool surface assuming that at each location, the atomic nitrogen partial pressures were consistent with dissociation temperatures which were 125 K higher than the local temperature. The physical modeling experiments reported in this paper show that the results of such studies can be applied, to quantitatively understand, albeit approximately, nitrogen concentrations in the weld metal.

Acknowledgments

This work was supported by the United States Department of Energy, Office of Basic Energy Sciences, Division of Materials Science, under Grant No. DEFG02-84ER45158. The authors are thankful to Dr. K. Mundra and Dr. S. A. David for their helpful comments. Mr. T. A. Palmer would also like to acknowledge financial support provided by the American Welding Society Foundation in the form of an AWS Graduate Research Fellowship.

References

1. Kou, S. 1987. *Welding Metallurgy*. pp. 61–63, New York , John Wiley and Sons.

2. Pehlke, R. D. 1979. *Unit Processes in Extractive Metallurgy*. pp. 141–145, New York, Elsevier.

3. Ohno, S., and Uda, M. 1981. Effects of hydrogen and nitrogen on blowhole formation in pure nickel at arc welding and non-arc melting. *Trans. Nat. Res. Inst. Met.* 23(4): 243–248.

4. Uda, M., and Ohno, S. 1978. Spattering phenomenon for iron-nitrogen system during arc melting. *Trans. Nat. Res. Inst. Met.* 20(6): 358–365.

5. Katz, J. D., and King, T. B. 1989. The kinetics of nitrogen absorption and desorption from a plasma arc by molten iron. *Metall. Trans.* B 20B: 175–185.

6. Bandopadhyay, A., Banerjee, A., and DebRoy, T. 1992. Nitrogen activity determination in plasmas. *Metall. Trans.* B 23B: 207–214.

7. den Ouden, G., and Griebling, O. 1990. Nitrogen absorption during arc welding. *International Trends in Welding Science and Technology*. eds. S. A. David and J. M. Vitek, pp. 431–435. ASM International, Materials Park, Ohio.

8. Lakomskii, V. I., and Torkhov, G. F. 1969. Absorption of nitrogen from a plasma by liquid metal. *Soviet Physics —Doklady* 13(11): 1159–1161.

9. Gedeon, S. A., and Eagar, T. W. 1990. Thermochemical analysis of hydrogen absorption in welding. *Welding Journal* 69: 264-s to 217-s.

10. Eliott, F., and Gleiser, M. 1963. *Thermochemistry for Steelmaking I*, p. 75, Reading, Mass., Addison-Wesley Publishing Co.

11. McGannon, H. E., ed. 1971. *The Making, Shaping and Treating of Steel*, 9th edition, pp. 330–331, US Steel Corp.

12. Dunn, G. J., and Eagar, T. W. 1986. Metal vapors in gas tungsten arcs: part II. theoretical calculations of transport properties. *Met. Trans. A* 17A: 1865–1871.

13. Moore, C. E. 1971. *Atomic Energy Levels*, Vol. 1–3, NSRDS-NBS 35, NBS, Washington, D.C.

14. Peebles, H. C., and Williamson, R. L. 1987. The Role of the Metal Vapor Plume in Pulsed Nd:YAG Laser Welding on Aluminum 1100. Proceedings of LAMP '87. pp. 19-24.

15. Shaw, C. B., Jr. 1975. Diagnostic studies of the GTAW arc. *Welding Journal* 54(2): 33-s to 44-s.

16. Collur, M. M., and DebRoy, T. 1989. Emission spectroscopy of plasma during laser Welding of AISI 201 Stainless Steel. *Metall. Trans B* 20B: 277–285.

17. Miller, R., and DebRoy, T. 1990. Energy absorption by metal-vapor-dominated plasma during carbon dioxide laser welding of steels. *J. Appl. Phys* 68 (5): 2045–2050.

18. Cecchi, J. L. 1990. *Handbook of Plasma Processing Technology*. eds. S. M. Rossnagel, J. J. Cuomo, and W. D. Westwood, pp. 15–16, Noyes Publications, Park Ridge, N.J.

19. Mitra, S. K. 1953. Active nitrogen. *Phys. Rev.* 90: 516–522.

20. Mundra, K., and DebRoy, T. 1995. A general model for partitioning of gases between a metal and its plasma environment. *Metall. and Mat. Trans.* 26B: 149 to 157.

21. Kuwana, T., and Kokawa, H. 1986. The nitrogen absorption of iron weld metal during gas tungsten arc welding. *Trans. of the Japan Weld. Soc* 17(1): 20–26.

22. Khan, P. A. A. 1987. Mass Transfer during Laser Welding of High Manganese Stainless Steels. pp. 72–74, Ph.D. thesis. University Park, Pa., The Pennsylvania State University.

23. DebRoy, T., and David, S. A. 1995. Physical processes in fusion welding. *Reviews of Modern Physics* 67 (1): 85–112.

24. David, S. A., and DebRoy, T. 1992. Current issues and problems in welding science. *Science* 257: 497– 502.

25. Bunshah, R. F., Blocher, J. M., Jr., *et al.* 1982. *Deposition Technologies for Films and Coatings: Developments and Applications*, p. 41. Noyes Publications, Park Ridge, N.J.

26. Banerjee, A., and DebRoy, T. 1992. Optical emission investigation of the plasma enhanced chemical vapor deposition of silicon oxide films. *J. Vac. Sci. Technol.* A 10 (6): 3395–3400.

27. Key, J. F., McIlwain, M. E., and Isaacson, L. 1980. *Sixth International Conference on Gas Discharges and Their Applications*, Pub. No. 189, Part 2, pp. 235–236, Institution of Electrical Engineers, New York, N.Y.

28. Olsen, H. N. 1959. Thermal and electrical properties of an argon plasma. *Physics of Fluids* 2(6): 614–623.

29. Holbert, R. K., Jr., Mustaleski, T. M., Jr., and Frye, L. D. 1987. Laser beam welding of stainless steel sheet. *Welding Journal* 77 (8): 21–25.

30. McKay, J. A., *et al.* 1979. Pulsed-CO_2-laser interaction with aluminum in air: thermal response and plasma characteristics. *J. Appl. Phys* 50(5): 3231–3240.

31. Rockstroh, T. J., and Mazumder, J. 1987. Spectroscopic studies of plasma during CW laser materials interaction. *J. Appl. Phys* 61(3): 917–923.